International Journal of Mechanical, Industrial and Aerospace Sciences
ISSN: 2517-9950
Vol:5, No:12, 2011

Novel Direct Flux and Torque Control of Optimally designed 6 phase Reluctance machine with special Current Waveform

E T. Rakgati and E. Matlotse

***Abstract*—**In this paper the principle, basic torque theory and design optimisation of a six-phase reluctance dc machine are considered. A trapezoidal phase current waveform for the machine drive is proposed and evaluated to minimise ripple torque. Low cost normal laminated salient-pole rotors with and without slits and chamfered poles are investigated. The six-phase machine is optimised in multi-dimensions by linking the finite-element analysis method directly with an optimisation algorithm; the objective function is to maximise the torque per copper losses of the machine. The armature reaction effect is investigated in detail and found to be severe. The measured and calculated torque performances of a 35 kW optimum designed six-phase reluctance dc machine drive are presented.

***Keywords*—**Reluctance dc machine, current waveform; design optimisation; finite element analysis; armature reaction effect.

I. Introduction

THIS paper focuses on high phase number reluctance machine drives with salient pole rotors. These drives have the advantage in high power (MW), high speed and bad environment applications for the petrochemical and mining industry amongst others. With a high phase number drive the current per phase is reduced without an increase in voltage per phase, which is important in high power drives. Salient pole reluctance rotors with no internal flux barriers are robust, maintenance free rotors that can be used at high speeds and in environments where any arcing within the machine is not allowed. In 1984 Weh [1] proposed a 6-phase reluctance dc machine drive with square-wave current waveforms and a salient-pole rotor. The research was followed-up by [2] and [3] using square-wave current waveforms for 5- and 7-phase machines and axially laminated salient-pole rotors. In these drives the phase windings act alternately as field or torque windings with dc currents, hence defined in this paper as reluctance dc machine (RDCM) drives.

In further developments on high phase number reluctance machine drives with salient pole rotors, important research was done by [4 - 8] on 5-phase sinusoidal reluctance synchronous machine (RSM) drives with the addition of third harmonic phase currents; hence defined in this paper as 5-phase+3rd RSM drives. The research shows that with the addition of third harmonic phase currents an increase in torque per *rms*-ampere is obtained.

E.T. Rakgati is a lecturer of Electric Machines & Drives at the University of Botswana, P/Bag UB 61 Gaborone, Botswana (phone: +267 355 4317; fax: +267 3952309; e-mail: rakgatie@mopipi.ub.bw).

E.Matlotse is a lecturer of Power Systems at the University of Botswana, P/Bag UB 61 Gaborone, Botswana (phone: +267 355 4338; fax: +267 3952309; e-mail: matlotsee@mopipi.ub.bw).

In this paper the 6-phase RDCM drive is further investigated with special attention to the current waveform, rotor structure, finite element (FE) design optimisation, torque-per-copper-loss performance and armature reaction effect. The rotor structure investigated is that of a normal laminated salient-pole type of rotor with or without slits and chamfered poles. The torque performance of the RDCM drive is also compared with that of a same stack volume, optimally designed 5-phase+3rd RSM. The FE calculated results are compared in the paper with measured results of a 4-pole, 35 kW, 230 Nm optimum designed 6-phase RDCM drive. As a first study, the paper does not focus on aspects like iron losses, power factor and efficiency.

II. Principle and RDCM torque

Consider a 2-pole, 6-phase RDCM with salient pole rotor as shown in Fig. 1. At the particular rotor position shown, phase winding coils $d-f$ act as field coils producing the flux in the machine, while phase winding coils $a-c$ as current conducting coils in a magnetic field act as torque coils.

The operation principle of the machine is such that the phase windings alternate as field or torque windings depending on the position of the rotor. Acting as a phase winding or a torque winding, dc current is forced into the winding as shown in Fig. 2 as proposed by Weh [1, 2]. The figure shows the field and torque current components I_F and I_T respectively of the current waveform.

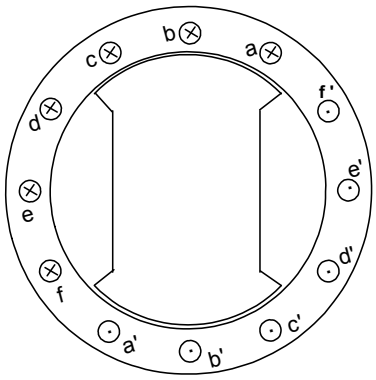

Fig. 1 Six-phase RDCM with salient pole rotor

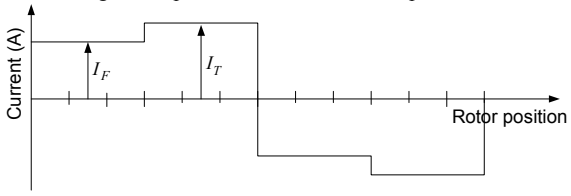

Fig. 2 Square current waveform for six-phase RDCM [1]

The developed torque of the RDCM as derived from the Lorentz force law can be expressed as

$$T = m_t \, k \, \varphi \, I_T \ , \tag{1}$$

where m_t is the number of torque producing phases, I_T is the torque producing current and k and φ are respectively a machine constant and the flux per pole given by

$$k = \frac{2 z q p}{\theta_r \, n_a} \qquad \varphi = B_g \, r \, l \, \theta_p \, , \tag{2}$$

In (2), θ_p is the rotor pole angle in radians, q is the number of slots per pole per phase, z is the number of conductors per slot, n_a is the number of parallel paths and p is the number of pole pairs. Furthermore B_g is the average airgap flux density, r is the radius of the airgap and l is the length of the stack. B_g and φ are calculated through FE analysis as will be explained later.

III. Effect of Current Waveform

Instead of the square current waveform of Fig. 2 a trapezoidal current waveform is proposed for the RDCM as shown in Fig. 3. The effect of these two current waveforms is first investigated by performing simplified airgap MMF analysis. In this analysis only the field current and, thus, only field MMF are considered, i.e. the torque current I_T is zero. Concentrated, full-pitch phase windings with rectangular airgap MMFs are furthermore assumed in the analysis. To simplify the analysis even more only the fundamental components of the rectangular phase MMFs are considered. The fundamental phase MMF of the *j-th* phase can be expressed in phasor notation by

$$\vec{F}_{j1}(\theta) = F_{j1\,peak}(\theta) \angle - n\delta \, , \tag{3}$$

where $j = a,b,...,f$ with corresponding $n = 0,1,2,...,5$, and $\delta = 180/m$ with m the number of phases, and

$$F_{j1\,peak}(\theta) = \frac{4}{\pi} \frac{N}{2} i_j(\theta) \, . \tag{4}$$

In (4) N is the number of turns per phase winding coil and $i_j(\theta)$ is the phase winding current as a function of rotor position. The resultant field MMF is obtained by taking the MMF phasor sum as

$$\vec{F}_1 = \sum \vec{F}_{j1}(\theta). \tag{5}$$

Using (5), the rotating field airgap MMFs with square and trapezoidal field current waveforms are determined, with the results shown in Figs. 4 and 5. It is clear that the square current waveform produces, as expected, a step-rotating MMF, while the trapezoidal field current waveform produces a continuous rotating MMF. Although the above MMF analysis is an approximation, the results of Figs. 4 and 5 clearly indicate that a smoother torque will be generated by the machine with the trapezoidal current waveform.

The effect of the square and trapezoidal current waveforms is further investigated by looking at the generated torque versus position of the RDCM. Note that in this paper only skewed reluctance machines are considered. The effect of skew is accounted for in the 2-D FE analysis by using a set of unskewed machines of which the rotors are relatively displaced by an angle that is a fraction of the total skew. This technique is explained amongst others by [9] and is also used in section V. With k_s unskewed machines the torque is calculated by

$$T_{skew} = \frac{1}{k_s} \sum_{i=1}^{k_s} T_i \, , \tag{6}$$

where T_i is the torque of the *i-th* unskewed machine determined by the Maxwell stress tensor method using a macro airgap element [10]. The results of the torque calculation for a skewed RDCM for both current waveforms are shown in Fig. 6. It is clear that the trapezoidal current waveform generates less ripple torque, with the average torque the same. Note in this case that the copper losses in the machine are the same for both current waveforms.

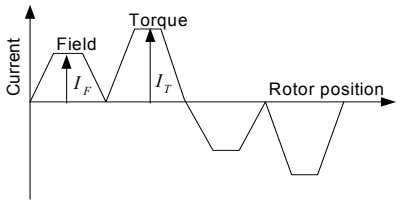

Fig. 3 New proposed trapezoidal current waveform with field and torque current components

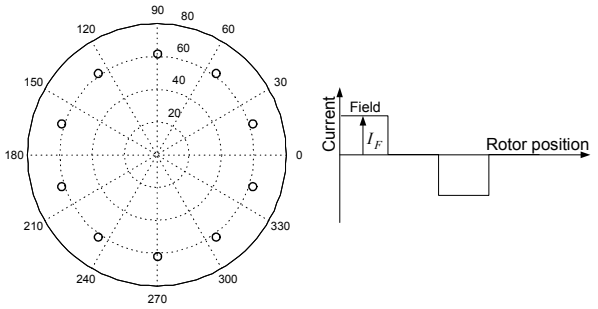

Fig. 4 Rotating field MMF plot with square field current waveform

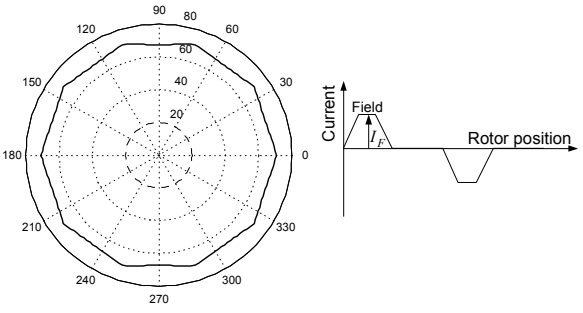

Fig. 5 Rotating field MMF plot with proposed trapezoidal current waveform

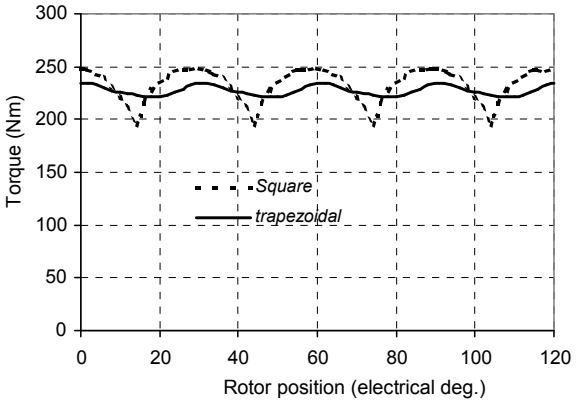

Fig. 6 Torque profiles of six-phase RDCM with trapezoidal and square current waveforms and skewed rotor

IV. Design Optimisation

In the design optimisation the non-gradient optimisation algorithm proposed by Powell [11] is used. The aim of the design optimisation is to maximise without any constraints the torque per copper losses per given stack volume of the 6-phase RDCM. The objective function for the unconstrained optimisation problem can simply be written as

$$Y = \mathbf{F(X)} = T\mathbf{(X)} \tag{7}$$

where X is a matrix vector representing the machine dimensions and other variables to be optimised, and $T(\mathbf{X})$ is the torque objective function to be maximized and Y is the output function value. The optimisation algorithm, thus, finds the multidimensional vector $\mathbf{X}$ that minimises Y of (7). In the optimisation procedure the FE solution is used directly by the optimisation algorithm. Each time the algorithm needs an output function value Y (torque value) for a given multidimensional input vector $\mathbf{X}$ (machine dimensions and other variables), it calls the FE program.

The FE program generates a new mesh according to the changed dimensions and then does the pre-processing and the nonlinear solution to find the magnetic vector potentials. From this the torque as the output function value Y of (7) is calculated according to (6) for the skewed machine. The FE program may be called a number of times by the optimisation algorithm during an iteration. At the end of each iteration a test is carried out to determine if an absolute maximum has been reached; if not a next iteration is executed. In this way the torque of the machine is maximised. It must finally be noted that the optimization is carried out on the fundamental (first harmonic or average) torque of the machine at a certain rotor position.

The machine under investigation is a 6-phase reluctance machine with a normal full-pitch stator winding with two slots per pole per phase as shown in Fig. 7. The rotor structure is a salient-pole rotor with no internal flux barriers as shown in Fig. 8. The dimensions to be optimised are also shown in Figs. 7 and 8. These are the stator yoke height, s_{yh}, the stator inner diameter, d_i, the tooth width, t_w, the rotor cut-out depth, r_c, the rotor cut-out angle, $\sigma=\theta_p/2$, and the ratio of the field current to torque current, I_F/I_T. With the field current I_F as an optimisation variable, the torque current I_T is calculated by

$$I_T = \sqrt{\frac{3P_{cu} - 5I_F^2 r_s}{5r_s}}\,, \tag{8}$$

where P_{cu} is the constant copper losses in the optimisation, and r_s is the per phase stator resistance calculated according to, amongst other things, the slot dimensions and conductor insulations. Note that the shaft diameter, d_{sh}, is kept constant in the design optimisation. The rotor outer diameter, d_r, is varied with the stator inner diameter, d_i, as the airgap length is kept constant in the optimisation.

The design optimisation results of the 6-phase RDCM are given in Table 1. Also given are the design optimisation results, found by [12], of a 5-phase+3rd RSM with the same amount of copper losses and stack volume as the RDCM. From these results it can be seen that the optimum dimensions of both machines are very much the same. Two remarkable results from the optimisation are (i) the relatively small rotor pole angle σ, probably to reduce the armature reaction effect, and (ii) the I_F/I_T-ratio of close to unity for the RDCM; this implies that the field current is closely equal to the torque current. Finally, in Table 1 the developed average torques of the optimally designed machines per rated copper losses are given. This shows that the skewed, 6-phase RDCM yields slightly (1.3%) higher torque than the skewed, 5-phase+3rd RSM.

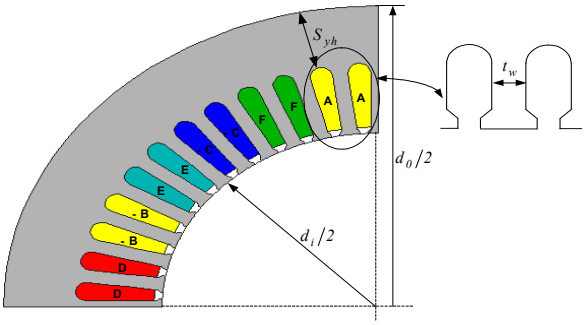

Fig. 7 Stator configuration (quarter section) of 6-phase RDCM

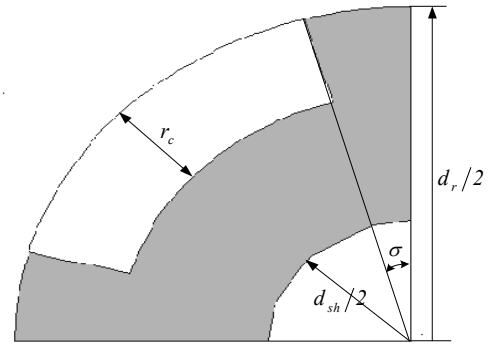

Fig. 8 Rotor structure (quarter section) of RDCM

TABLE I
OPTIMISATION RESULTS

Fix parameters	6-phase RDCM	5-phase+3rd RSM [12]
P_{cu} (kW)	2	2
airgap (mm)	62	62
d_o (mm)	340	340
stack length (mm)	175	175
d_{sh} (mm)	70	70
Variables	6-phase RDCM	5-phase+3rd RSM [12]
t_w (mm)	6.9	8.2
s_{yh} (mm)	32.4	32.9
d_i (mm)	196.1	194.3
r_c (mm)	23.3	25.1
$\sigma=\theta_p/2$ (°)	16.2	15.6
I_F/I_T	0.87	-
Current angle (°)	-	56.7
Torque (Nm)	227.7	224.8
Torque (p.u.)	1.0	0.987

V. ARMATURE REACTION EFFECT

The armature reaction effect, as in brush dc machines, is investigated by studying the variation of the airgap flux at different positions of the salient pole rotor. Figure 9 shows a layout of the skewed rotor pole represented by k_s=5 unskewed and displaced rotor poles; the skew angle is β. Also shown is the expected average airgap flux density across the axial length of the rotor pole. The airgap flux density with skew taken into account is calculated by

$$B_g(\theta)=\frac{1}{k_s}\sum_{i=1}^{k_s} B_{gi}(\theta), \qquad (9)$$

$\theta)$ is the radial component of the airgap flux density of the *i-th* unskewed machine determined by

$$B_{gj}(\theta)=\frac{2}{d_i}\left(\frac{A_{z(j+1)}-A_{zj}}{\theta_{j+1}-\theta_j}\right), \qquad (10)$$

where A_{zj} is the known vector potential of the *j-th* node at the inner stator diameter of the machine. To study the armature reaction effect the rotor pole is divided into three pole sections as shown in Fig. 9. For each *n-th* pole section the flux per pole section φ_n is determined as

$$\varphi_n = B_{gn}\, r\, l\, \alpha\ , \qquad (11)$$

where B_{gn} is the average flux density of the *n-th* pole section obtained by averaging the $B_g(\theta)$ of (9) across the pole section angle $\alpha = (\theta_p + \beta)/3$.

The results of the averaged (filtered) airgap flux density andflux per pole section of the RDCM of Figs. 7 and 8 and Table 1 under no-load (only rated field current) and full-load (rated field and rated torque current) conditions are shown in Figs. 10 and 11 respectively. It is clear that the armature reaction effect on the airgap flux density and flux per pole section is severe in this machine. This will have a negative effect on the torque performance of the machine, especially in the field weakening speed range.

To reduce the armature reaction effect of the 6-phase RDCM, two other rotor structures are investigated. These rotor structures have slitted and chamfered rotor poles as shown in Figs. 12(a) and (b) respectively. The idea of using slitted field poles to reduce the armature reaction effect is not new and was proposed already in 1904 by Thomson [13]. Furthermore, chamfering the field poles of brush dc machines to reduce armature reaction is common practice.To determine the torque performance and armature reaction effect with the slitted and chamfered rotors, the RDCM is re-optimised in its design as explained in section IV. Some of the optimisation results found, together with the optimum results of the standard rotor RDCM, are given in Table II. It can be seen that there is little difference in the optimum results of the RDCMs, with the only significance, maybe, the lower currents and lower I_F/I_T current ratio of the chamfered rotor RDCM. The torque performance results in Table II show that the slitted and chamfered rotors increase the torque of the RDCM by almost 6%, which is significant.The calculation of the flux per pole section according to (11) is repeated for the RDCM with the slitted and chamfered rotors. The results in Fig. 13 show clearly that the armature reaction effect is reduced with these rotors, which explains the improved torque performance found for the RDCM with these rotors.

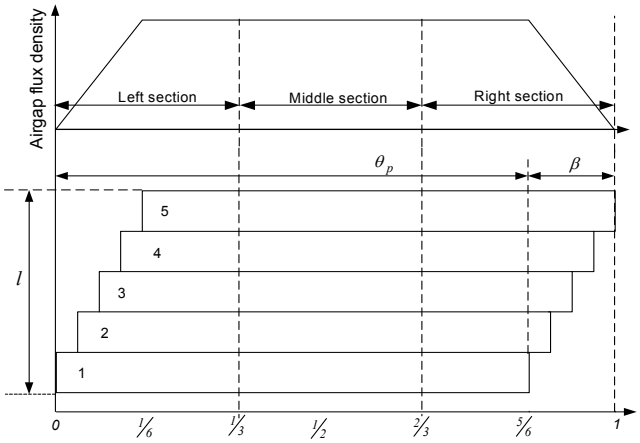

Fig. 9 Average airgap flux density across rotor pole, skew layout and pole sections

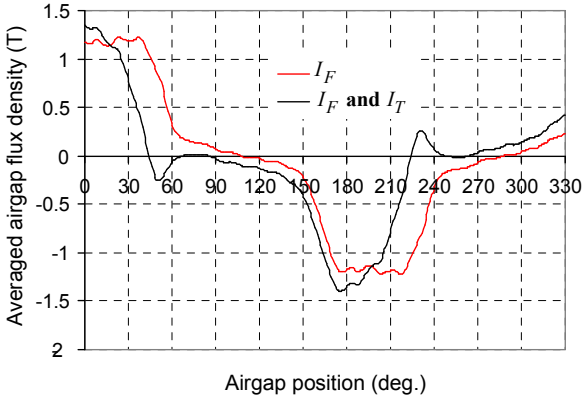

Fig. 10 Averaged (filtered) flux density of 6-phase RDCM with rated field current and with rated field and rated torque currents

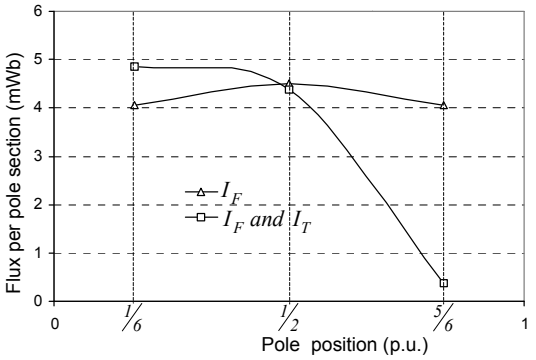

Fig. 11 Flux per pole section of 6-phase RDCM with rated field current and with rated field and rated torque currents

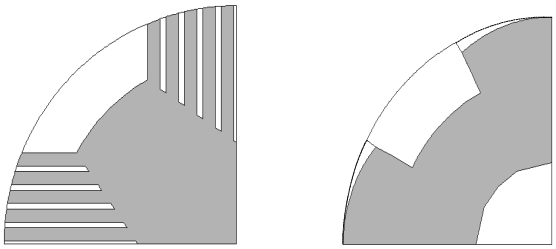

(a) (b)

Fig. 12 (a) Slitted and (b) chamfered rotor pole structures of RDCM

TABLE II
OPTIMUM DIMENSIONS AND TORQUE PERFORMANCE OF 6-PHASE RDCM WITH DIFFERENT ROTORS

Parameter	Standard rotor Fig. 8	Slitted rotor Fig. 11(a)	Chamfered rotor; Fig. 11(b)
s_{yh} (mm)	32.4	32.4	31.2
d_i (mm)	196.1	189.7	198.4
σ (°)	16.2	15.3	15.6
I_F (A)	39	39.5	36.8
I_T (A)	45	44.9	43.1
I_F/I_T	0.87	0.88	0.85
Torque (p.u.)	1.0	1.057	1.06
Torque – eqn (6)	227 Nm	240.1 Nm	240.5 Nm
Torque – eqn (12)	231.1 Nm	233.0 Nm	233.5 Nm

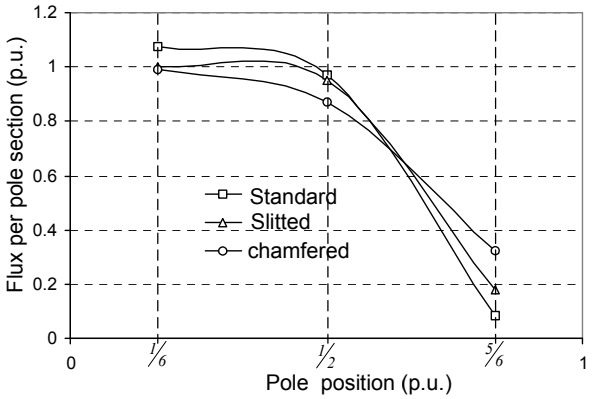

Fig. 13 Flux per pole-section of 6-phase RDCM with different rotor structures with rated field and rated torque currents

The torque of the optimum 6-phase RDCM with the different rotor structures is also calculated by (1) to compare the outcome with the FE Maxwell stress tensor torque calculation method of (6). For the skewed rotor RDCMs the torque is calculated according to (1) as

$$T = \xi\, k\, I_T \sum_{n=1}^{3} \varphi_n \ , \qquad (12)$$

where φ_n is calculated by (11) and θ_p in (2) is replaced by the angle $\theta_p+\beta$. In accounting for the torque ripple, the torque is averaged for two cases corresponding to two active torque phase windings ($\xi = 2$) and three active torque phase windings ($\xi = 1+(\theta_p+\beta-30)/2\beta$). The result of this calculation is given in Table II. It is clear that the torque calculated according (12), which is based on the Lorentz force law, gives very similar results as the FE calculated torque for the skewed rotor RDCM and hence can be used in analysis.

VI. CALCULATED AND MEASURED RESULTS

The optimally designed 6-phase RDCM with the skewed rotor was built and tested. A photo of the optimum designed skewed rotor of the RDCM is shown in Fig. 14.

For testing the machine, the drive system of Fig. 15 is used. The machine is controlled by a floating point DSP with current and position feedback and a 6-phase, full-bridge per phase inverter. The control block diagram of the system is shown in Fig. 16. The control is done in such a way that a constant field command current I_F^* is input to the system in the constant flux (sub-base) speed region, but a reduced field command current in the field weakening (high) speed region.

The torque command current I_T^* is controlled by the speed controller. As mentioned by [14], with non-sinusoidal current references a hysteresis current regulator is a more popular choice for current control. Hence, a hysteresis current regulator with a fixed band is digitally implemented for the RDCM drive. The measured phase current at no-load is shown in Fig. 17. There is a noticeable hysteresis band on the current waveform.

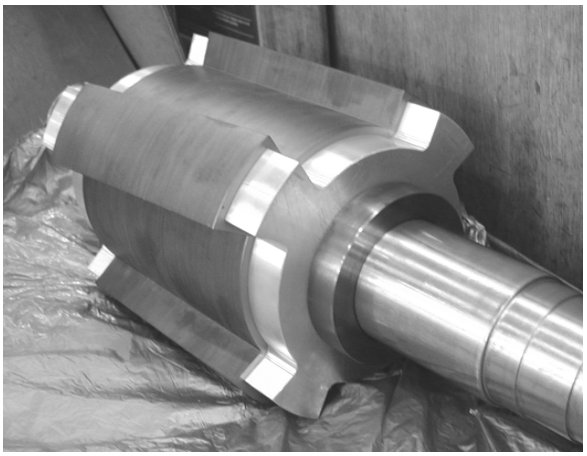

Fig. 14 Skewed rotor of 6-phase RDCM

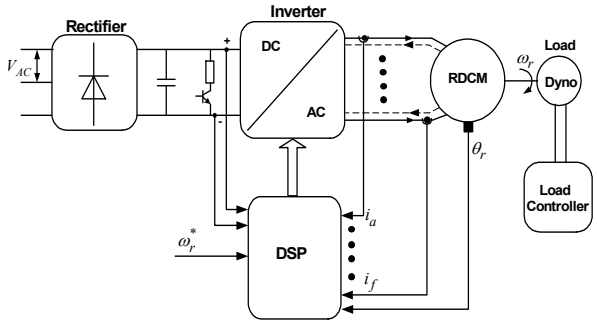

Fig. 15 Block diagram of 6-phase RDCM drive

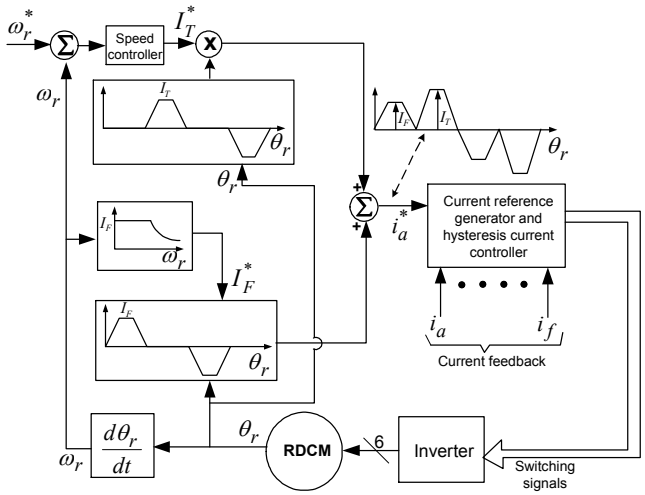

Fig. 16 Block diagram of the current controlled 6-phase RDCM

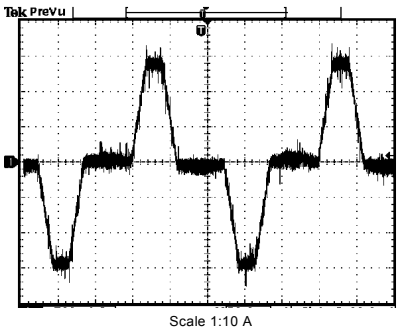

Fig. 17 Measured current waveform at no-load (I_F = 30 A and I_T = 0A)

The torque performance of the RDCM with different field currents is shown in Fig. 18. It is clear that the measured results do correspond accurately with the FE calculated results. Furthermore, it is clear that the armature reaction effect is severe under field weakening conditions; at rated field current a very-much linear relationship between torque and torque current is obtained.

The ripple torque of the RDCM is also investigated by static torque measurements. The results of the static torque measurements in comparison with FE calculated results are shown in Fig. 19; the static torque test is done at rated field and rated torque current. Again good correlation is found between calculated and measured results. The ripple torque is clearly caused by the phase current commutation every 30° electrical.

The performance of the RDCM in the field-weakening speed region is also investigated. For the field-weakening test the field is reduced with the terminal voltage and the torque current constant. The poor torque performance of the machine in the field-weakening speed region is shown in Fig. 20. This performance can be improved by the use of slitted or chamfered rotor poles as shown in the previous section.

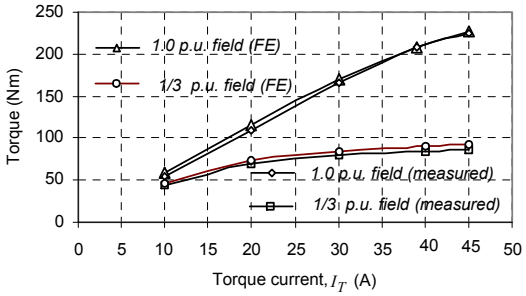

Fig. 18 Torque performance of 6-phase RDCM with different field currents

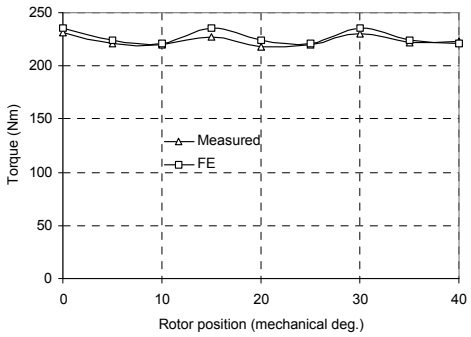

Fig. 19 Static torque versus position of 6-phase RDCM

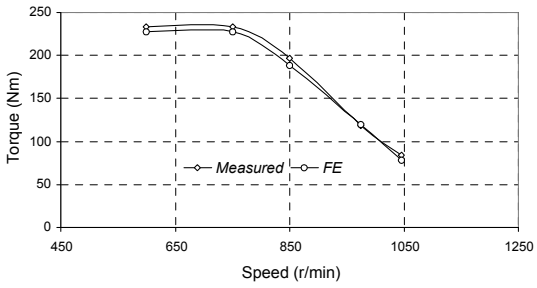

Fig. 20 Torque performance of the 6-phase RDCM in the field-weakening speed region

REFERENCES

[1] Weh H.: "Zur Weiterentwicklung wechselrichter-gespeister reluktanz-maschinen fur hohe leistungs-dichten und grobe leistung", ETZ Archiv, 1984, Vol. 6, No.4, pp. 135-141.

[2] Weh H. and Schroder U.: "Static inverter concepts for multiphase machines with square-wave current field distributions", European Power Electronic Conference (Brussels), 1985, pp. 1147-1152.

[3] Boldea I. and Nasar S.A.: "Emerging electric machines with axially laminated anisotropic rotors: A review", Electric Machines and Power systems, 1991, Vol. 19, pp. 673 – 701.

[4] Toliyat H.A, Xu L and Lipo T.A, "A five-phase reluctance motor with high specific torque", IEEE Transactions on IAS, Vol. 28, pp. 659 – 667, no.3, May/June 1992.
[5] Xu L, "Rotor structure selections of non-sine five-phase synchronous reluctance machines for improved torque capability", IEEE Transactions on IAS, vol. 36, no.4, pp. 1111 – 1117, July/August 1992.
[6] Toliyat H.A, Waikar P.S. and Lipo T.A, "Analysis and simulation of five phase synchronous reluctance machines including third harmonic of airgap MMF", IEEE Transactions on IAS, vol. 34, no.2, pp. 332 – 339, March/April 1998.
[7] Xu L and Fu W.N, "Evaluation of 3rd harmonic component effects in 5-phase synchronous reluctance motor drive using time stepping finite element method", IEEE IAS Conf. record , 2000, pp. 1– 8.
[8] Toliyat H.A, Shi R and Xu H, "A DSP-based vector control of five-phase synchronous reluctance motor", IEEE IAS Conf. record , 2000, pp. 1– 7.
[9] Bomela X.B., Kamper M.J.: "Effect of stator chording and rotor skewing on performance of reluctance synchronous machine", IEEE Trans. Ind. Appl. Soc. (IAS), vol. 38, no. 1, pp. 91-100, Jan. 2002.
[10] Abdel-Razek A.A., Coulomb J.L., Feliachi M. and Sabonnadiere J.C.: "The calculation of the electromagnetic torque in saturated electric machines within combined numerical and analytical solutions in the field equations", IEEE Trans. on Magnetics, vol. 17, no. 6, pp. 3250-3252, Nov. 1981.
[11] Powell M.J.D.: "An efficient method for finding the minimum of a function of several variables without calculating derivatives", Computer Journal, 1964, vol. 7, pp. 155-162.
[12] Rakgati E.T and Kamper M.J, "Torque performance of optimally designed three and five-phase reluctance synchronous machines with two rotor structures", Trans. SAIEE, on printing Dec. 2006.
[13] Thompson S.P.: "Dynamo electric machinery", M. Strong (New York, N.Y.), eighth edition, pp. 389 (Fig. 264), 1911.
[14] Manjrek M.D, Steimer P.K and Lipo T.A: "High multilevel power conversion system: A competitive solution for high power applications", IEEE Transactions on IAS, vol. 36, no.3, pp. 834– 841, May/June 2000.